Mitochondrial dysfunction and calcium dysregulation in COQ8A-Ataxia Purkinje neurons are rescued by CoQ 10 treatment

Ioannis Manolaras, Andrea del Bondio, Olivier Griso, Laurence Reutenauer, Aurélie Eisenmann, Bianca Habermann, Hélène Puccio

Mitochondrial dysfunction and calcium dysregulation in COQ8A-Ataxia Purkinje neurons are rescued by CoQ_{10} treatment

Ioannis Manolaras,[1-4] Andrea Del Bondio, [5-6] Olivier Griso,[1-4] Laurence Reutenauer,[1-6] Aurélie Eisenmann,[1-4] Débora Farina-Goncalves, [5-6], Fanny Fontaine,[7] Bianca H. Habermann,[8] and Hélène Puccio,[1-6] *

Abstract

COQ8A-Ataxia is a rare form of neurodegenerative disorder due to mutations in the *COQ8A* gene. The encoded mitochondrial protein is involved in the regulation of Coenzyme Q_{10} biosynthesis. Previous studies on the constitutive *Coq8a*$^{-/-}$ mice indicated specific alterations of cerebellar Purkinje neurons involving altered electrophysiological function and dark cell degeneration. In the present manuscript, we extend our understanding of the contribution of Purkinje neuron dysfunction to the pathology. By generating a Purkinje specific conditional COQ8A knockout, we demonstrate that loss of COQ8A in Purkinje neurons is the main cause of cerebellar ataxia. Furthermore, through *in vivo* and *in vitro* approaches, we show that COQ8A-depleted Purkinje neurons have abnormal dendritic arborizations, altered mitochondria function and intracellular calcium dysregulation. Furthermore, we demonstrate that oxidative phosphorylation, in particular Complex IV, is primarily altered at pre-symptomatic stages of the disease. Finally, the morphology of primary Purkinje neurons as well as the mitochondrial dysfunction and calcium dysregulation could be rescued by CoQ_{10} treatment, suggesting that CoQ_{10} could be a beneficial treatment for *COQ8A*-Ataxia.

Author affiliations:

1 Institut de Génétique et de Biologie Moléculaire et Cellulaire (IGBMC), 67404 Illkirch, France.

2 Inserm, U1258, 67404 Illkirch, France.

3 CNRS, UMR7104, 67404 Illkirch, France.

4 Université de Strasbourg, 67000 Strasbourg, France.

5 Institut Neuromyogène, Inserm U1315, 69008 Lyon, France.

6 CNRS, Université Claude Bernard Lyon I, UMR 5261, 69008 Lyon, France.

7

8 Aix-Marseille University, CNRS, Institut de Biologie du Développement de Marseille (IBDM), UMR7288, 13009 Marseille, France.

- Correspondence to: Hélène Puccio

Institut NeuroMyoGène, Unité Pathophysiologie et Génétique du Neurone et du Muscle (PGNM), UMR5261 INSERM U1315, Université Claude Bernard Lyon I, Faculté de Médecine, 8 avenue Rockefeller, 69008 Lyon France

helene.puccio@inserm.fr

Running title: CoQ10 treatment improves COQ8A-ataxia

Keywords: ataxia; Coenzyme Q10; Purkinje Neurons; mitochondria; calcium

Introduction

COQ8A-ataxia (former name: ARCA2, autosomal recessive ataxia type 2) is a rare recessive form of multisystemic ataxia characterized by slowly progressive early-onset ataxia, combined with variable features including exercise intolerance, epilepsy, intellectual disability and dystonia.[1–3] It is caused by biallelic loss of function mutations in *COQ8A* (former name: *ADCK3*).[1,2] Although the exact function of COQ8A remains unclear, it is a mitochondrial atypical kinase/ATPase, activated by CoQ_{10} precursors and lipids of the inner mitochondrial membrane.[4,5] COQ8A is required to ensure CoQ_{10} biosynthetic complex (Complex Q) integrity and has been suggested to regulate CoQ biogenesis.[5–7] Although variable, low CoQ_{10} levels have been identified in skeletal muscle and fibroblasts in some patients, and fibroblast lines derived from COQ8A-ataxia patients display defects in mitochondrial homeostasis and signs of oxidative stress.[3,8]

Although rare, COQ8A-ataxia is the most common form of primary CoQ_{10} deficiencies, a heterogeneous group of disorders ranging from severe infantile multisystemic disease to adult-onset isolated myopathy.[9,10] The phenotypic variability of primary CoQ_{10} deficiencies likely reflects cell-type-specific differences in COQ proteins expression, CoQ_{10} production, uptake, and/or demand. Despite the great heterogeneity, CoQ_{10} deficiency causes mitochondrial dysfunction in the affected tissues.[1] The closest paralog of COQ8A is COQ8B/ADCK4 whose mutations manifest as steroid-resistant nephrotic syndrome.[11] COQ8B has also recently been demonstrated to interact with Complex Q and be required for its integrity,[12] suggesting similar function to COQ8A.

We have previously generated a *Coq8a*$^{-/-}$ constitutive knockout (KO) mouse model that recapitulates most hallmarks of the human disease**,** including a mild progressive cerebellar ataxia, exercise intolerance, increased epileptic susceptibility and mild memory impairment.[4] *In vivo*, loss of COQ8A in mouse led to complex Q destabilization and a variable reduction of CoQ in skeletal muscle, liver and kidney.[4] We have demonstrated that COQ8A deficiency led to degenerating Purkinje Neurons (PN), with an alteration in the pacemaking activity.[4] Interestingly, 10-20% of PN were characterized by dark and shrunken morphology,[4] a specific type of cellular degeneration that has been associated with excitotoxicity and high levels of intracellular calcium (Ca^{2+}) in other forms of spinocerebellar ataxias.[13–15] By electron microscopy, while mitochondria appear structurally normal, most PN presented dilated and fragmented Golgi apparatus and dilated endoplasmic reticulum (ER). Interestingly, granule

cells (GC) did not show any morphological nor ultrastructural defects in the constitutive KO. These results suggest that the cerebellar ataxia might be linked specifically to PN degeneration. However, the cell specificity and the underlying molecular mechanism of the disease are unknown.

To address these questions, we have combined a variety of experimental approaches both *in vivo* and *in vitro* to uncover the molecular pathways underlying the disease mechanism in PN. We first showed that COQ8A is highly expressed in PN, whereas its closest paralog COQ8B is mostly expressed in GC. Furthermore, we demonstrated that specific deletion of COQ8A in PN was sufficient to cause ataxia in a conditional mouse model. Moreover, we uncovered that *Coq8a*$^{-/-}$ PN *in vivo* and *in vitro* exhibited first mitochondrial dysfunction followed by Ca^{2+} deregulation. Finally, with the aim to develop a therapeutic strategy, we demonstrated that PN morphology, mitochondrial function and Ca^{2+} homeostasis could be rescued by CoQ_{10} treatment *in vitro*. These results allow to better understand the molecular pathways involved in the cerebellar pathophysiology of *COQ8A*-ataxia and provide strong rational for using CoQ_{10} analogs as a possible treatment.

Materials and methods

Mice and cell culture

Coq8a$^{-/-}$ mice deleted for exons 9–14 were generated by homologous recombination as previously reported.[4] *Pcp2-Cre;Coq8a* $^{L2+/L2+}$ mice were generated by crossing conditional *Coq8a* $^{L2+/L2+}$mice with *Pcp2-Cre* expressing mice. Housing animal facility was controlled for temperature and humidity, with a 12 hours light/dark cycle and free access to water and a standard rodent chow (D03, SAFE, Villemoisson-sur-Orge, France). All animal procedures and experiments were approved by the local ethical committee for Animal Care and Use (APAFIS#4217-2016022318157919). They were performed in accordance with the Guide for the Care and Use of Laboratory Animals (National Institutes of Health).

Accelerating Rotarod

Coordination, balance, and motor skill acquisition were tested using an accelerating rotating rod (Panlab, Barcelona, Spain) test as described previously.[4] Briefly, mice were placed on the rod in 4 trials every day for a period of 4 days (12 WT and 12 *Pcp2-Cre;Coq8a*$^{L+/L+}$ mutants). The rod accelerated from 4 rpm to 40 rpm in 5 min and remained at maximum speed for the next 5 min. Animals were scored for their latency to fall for each trial and rested a minimum of 10 min between trials to avoid fatigue. Results were analyzed by a repeated-measure ANOVA test considering three factors: days (fixed); genotype (fixed); animals (variable), nested in genotype and crossed with days.

Footprint Analysis (Linear Movement)

The test was performed as previously described.[16] Briefly, after coating of the hind and front feet with nontoxic ink, mice were allowed to walk through a tunnel (50×9×6 cm) with paper lining the floor. Three parameters were quantified: linearity, average change in angle between consecutive right-right steps. A high linearity score is indicative of nonlinear movement. Matching of left and right steps, the overlap of hind and front paws.

Primary Cerebellar cultures

Primary cerebellar cultures were generated from P0 Ctrl and constitutive *Coq8a*$^{-/-}$ cerebellum by modifying the number of plated PN to 10^6 / well (24-well plates were used) of a previously described protocol.[15,17]. For the rescue of *Coq8a*$^{-/-}$ primary cultures, 10 μM of CoQ_{10} were added from day DIV2 until DIV21.

Immunofluorescence, histo-enzymatic staining, electron and live imaging microscopy

Immunofluorescence

Whole brains from mice were extracted and fixed in 4% PFA over-night (ON). Brains were cryoprotected in 30% sucrose in PBS for 48 hours, snap frozen in dry ice-cold isopentane and embedded in OCT. Sections of 30μm were cut using Cryostat and floating IHC protocol was followed as previously described.[18,19] The primary antibodies (all used at 1/250 dilution) were against**:** COQ8A (generated in-house against the peptide KQMTKTLNSDLGPHWRDKC), anti-GAPDH (1/40000, Millipore, MAB374), COQ7 (Santa Cruz, sc-376484), COQ5 (Proteintech, 17453-1-AP), COQ8B (generated in-house against the peptide PGGSLQHEGVSGLGC), CALB1 (Sigma-Aldrich, C9848), COXIV (Proteintech, 11242-1-AP), IP3R1 (Novus biologicals, NBP1-21398), and vGLUT2 (Millipore, AB2251). Images were acquired using SP5 confocal and spinning disk LEICA microscopes and treated with ImageJ.

Electron Microscopy

Electron microscopy was performed as followed: Briefly, animals were intracardiac perfused with 4% PFA. Tissues were fixed in 2.5% glutaraldehyde in PBS. After overnight fixation, tissues were rinsed in PBS, postfixed in 1% osmium tetroxide-PBS (2 hr, 4 °C), dehydrated, and embedded in Epon. Regions of interest were localized on 2 μm sections and stained with toluidine blue. Ultrathin sections from selected areas were stained with uranyl acetate and lead citrate and examined with a Philips 208 electron microscope, operating at 80 kV.

Live imaging

Primary cerebellar cultures at DIV21 were imaged using live fluorescence microscopy to determine mitochondrial membrane potential (by TMRM; T668, Thermofisher), oxidative

stress (by MitoSOX™; M36008 Thermofisher), and calcium homeostasis (by Calbryte520TM AAT; Bioquest). All the probes were used based on the manufacture's protocols.

Histo-enzymatic staining of ETC complexes I, II, and IV

The protocol used has been previously described here.[20] Briefly, cerebellum from 5-30 weeks old mice were frozen embedded in O.C.T, and serial sections of 14 µm thick were performed on a cryostat. The sections were incubated for 40 min at 37 °C in freshly prepared appropriate complex histochemistry media:

For complex I, 1.23 mg/ml, (1.5 mM) Nitroblue tetrazolium (NBT; N6876, Sigma) and 0.625 mg/ml NADH (N8129, Sigma) were mixed in PBS, pH=7.4.

For complex II, 1.23 mg/ml, (1.5 mM) NBT, 35.12 mg/ml (130 mM) sodium succinate (S2378, Sigma), 0.0613 mg/ml (0.2 mM) Phenazine methosulfate (PMS; P9625, Sigma) and 0.065 mg/ml (1 mM) sodium azide (S8032, Sigma) were mixed in PBS.

For complex IV, 0.5 mg/ml 3,3′-diaminobenzidine Tetrahydrochloride (DAB, D7304, Sigma), 1 mg/ml cytochrome c (C2506, Sigma) and 2 µg/ml bovine catalase (C9322, Sigma) were mixed in PBS, pH =7.4.

For primary culture stainings, cells were pre-incubated with 0,2 U/ml Streptolysin O for 10 min at 37°C and then appropriate complex histochemistry media were added.

Antibodies and Western Blots

Western blots were performed according to standard protocol, including separation of proteins by SDS Tris-Glycine PAGE. Antibodies were diluted as follows: anti-COQ8A (IGBMC), anti-GAPDH (1/40000, Millipore), anti-COQ7 (1/1000, Santa cruz), anti-COQ5 (Proteintech

17453-1-AP, 1/1000), IP3R1 (Novus biologicals 1/1000), CAMKIIα (GeneTex, GTX133071 1/1000), p-CAMKIIα (ABclonal, AP0255 1/1000), EAAT4 (Abcam 1/1000), EAAT1 (Abcam 1/1000), vGLUT2 (Millipore 1/3000), vGLUT1 (GeneTex, GTX54870 1/3000), vGAT (Santa Cruz, sc-393373 1/1000).

Laser Capture Microdissection (LCM) coupled to RNA-seq

Full length cDNA was generated from 1500 pg of total RNA using Clontech SMART-Seq v4 Ultra Low Input RNA kit for Sequencing (Takara Bio Europe, Saint Germain en Laye, France) according to manufacturer's instructions with 11 cycles of PCR for cDNA amplification by Seq-Amp polymerase. 600 pg of pre-amplified cDNA were then used as input for Tn5 transposon tagmentation by the Nextera XT DNA Library Preparation Kit (Illumina, San Diego, CA) followed by 12 cycles of library amplification. Following purification with Agencourt AMPure XP beads (Beckman-Coulter, Villepinte, France), the size and concentration of libraries were assessed by capillary electrophoresis. Libraries were then sequenced on an Illumina HiSeq4000 sequencer as single-end 1x50 base reads.

Image analysis and base calling were performed using RTA 2.7.7 and bcl2fastq 2.17.1.14. Reads were preprocessed using cutadapt[21] version 1.10 in order to remove adapter, polyA and low-quality sequences (Phred quality score below 20), reads shorter than 40 bases were discarded for further analysis. Reads mapping to rRNA were also discarded (this mapping was performed using bowtie version 2.2.8).[22] Reads were then mapped onto the mm10 assembly of mouse genome using STAR version 2.5.3a.[23] Gene expression was quantified using htseq-count version 0.6.1p1 and gene annotations from Ensembl release 94.[24] Statistical analysis was performed using R 3.3.2 and DESeq2 1.16.1 Bioconductor library.[25] Only non-ambiguously assigned reads have been retained for further analyses.

Quantitative RT-qPCR

Total RNA was extracted from frozen tissues with the Precellys homogeniser (Bertin Technologies) and using TRI Reagent (MRC) according to the manufacturer's protocol. cDNA was generated by reverse transcription using the Transcriptor First strand cDNA synthesis kit (Roche). Quantitative RT-PCR was performed using the SYBR Green I Master (Roche) and light Cycler 480 (Roche) with the primers described below. *Gapdh* or *Hprt* was used as internal standard for the quantification. Primers: *cox4i1* F-TGAATGGAAGACAGTTGTGGG, R-GATCGAAAGTATGAGGGATGGG, *cox5b* F-ACCCTAATCTAGTCCCGTCC, *Cox6a2,* RCAGCCAAAACCAGATGACAG, *Uqcrq* F-GTGATCTCCTACAGCTTGTCG, R-CCCATGTGTAGATCAGGTAGAC, *Ndufa7* F-GCTACTCGCGTTATCCAAAAG, R-TGTTGGACAGCTTGTGACTG, *Hprt* F-GTAATGATCAGTCAACGGGGGAC, R-CCAGCAAGCTTGCAACCTTAACCA

Data Availability

The data that support the findings of this study are available within the article and its supplementary material. The raw RNA seq data are deposited on the GEO NCBI repository site.

Results

COQ8A depletion in PN leads to cerebellar ataxia and PN degeneration

We have previously shown specific morphological and functional defects in cerebellar PN in *Coq8a*$^{-/-}$ mice.[4] Consistent with our previous observations of abundant *Coq8a* mRNA in PN,[4] immunofluorescence experiments on wild-type cerebellar slices showed a specific COQ8A expression pattern in the cerebellum, with high expression levels in PN (Figure 1A). In

addition, while no expression of COQ8A was seen in GC, low levels of expression was observed in mossy fibers rosettes in the GC layer (Figure 1A). The specificity of the antibody was validated by the complete absence of staining in the *Coq8a*$^{-/-}$ cerebellum (Figure 1A,E). Similar to COQ8A, high expression of COQ7 and COQ5 was observed in PN as well as in the mossy fibers rosettes (Figure 1B-C). As previously demonstrated by proteomic and western blot analysis,[4] a strong decrease in COQ7 and COQ5 staining was observed in the *Coq8a*$^{-/-}$ cerebellum (Figure 1B-C,E). In contrast to COQ8A, its closest paralog COQ8B was not detected in PN while it was highly expressed in GC (Figure 1D). Furthermore, no compensatory COQ8B expression was seen in the *Coq8a*$^{-/-}$ cerebellum (Figure 1D,E).

Considering the specific expression pattern of COQ8A in the cerebellum, we sought to determine whether PN-specific deletion of COQ8A was sufficient to cause cerebellar ataxia. We thus generated a conditional KO mouse model deleted for COQ8A specifically in PN (*Pcp2-Cre;Coq8a*$^{L+/L+}$) (Supplementary Figure 1). To assess the neurological consequences of COQ8A depletion in PN, we conducted behavioral analyses. By 20 weeks of age, both males and females *Pcp2-Cre;Coq8a*$^{L+/L+}$ mice showed decreased performance on accelerating rotarod (Figure 2A). Moreover, footprint analysis showed increased in non-linear movement and decreased overlap of hind and front limbs at 20 weeks of age, features characteristic of ataxia (Figure 2B). Similarly to the constitutive *Coq8a*$^{-/-}$ mice,[4] *Pcp2-Cre;Coq8a* $^{L+/L+}$ mice showed specific defects in the cerebellar PN layer, with the presence of shrunken neurons and patches of gaps in calbindin staining, suggesting neuronal degeneration (Figure 2C). Degenerating neurons were found throughout all cerebellar lobules but tend to be more pronounced in lobules 9 and 10. Together, these results demonstrate that PN-specific deletion of COQ8A leads to cerebellar ataxia with loss of coordination that precedes PN degeneration. However, it is likely that depletion of COQ8A in other cerebellar cells, such as the mossy fibers rosettes, other tissues such as skeletal muscle or that deletion of COQ8A during embryogenesis contribute to the cerebellar ataxia since the constitutive COQ8A knockout showed an earlier onset and more severe phenotype.[4]

To further investigate the pathological consequence of COQ8A depletion in PN, we generated primary cerebellar cultures from Control (Ctrl) and the constitutive *Coq8a*$^{-/-}$ P0 pups. These cultures although enriched in PNs, present abundant GCs and glial cells . As a first observation, after 21 days *in vitro* (DIV21), the number of PN in *Coq8a*$^{-/-}$ cultures was significantly lower compared to Ctrl cultures (Figure 2D). In addition, morphological analysis of PN indicated a lower complexity of dendritic arborizations in *Coq8a*$^{-/-}$ PN (Figure 2D-E). Specifically, the

number of primary dendritic nodes was found significantly lower in *Coq8a*$^{-/-}$ compared to the Ctrl PN (Figure 2E). However, no difference was observed in the thickness of the main dendrite between Ctrl and *Coq8a*$^{-/-}$ PN (Figure 2E). Furthermore, the surface area covered by each individual PN was comparable between the two genotypes (Figure 2E). Thus, COQ8A deficiency leads to a decrease survival of PN in primary cerebellar cultures and a decrease dendritic complexity in the surviving PN.

COQ8A deletion causes altered transcript expression related to OXPHOS in PN

To understand the early molecular signatures in *Coq8a*$^{-/-}$ animals, bulk RNA sequencing analysis was performed after laser capture microdissection (LCM) of PN layer as well as GC layer from 5 weeks old animals. The number of deregulated genes was considerably higher in *Coq8a*$^{-/-}$ PN (330) compared to GC (17) (Figure 3A and Supplementary Tables 1-2), with only 7 transcripts overlapping, further validating the specific role of PN in the pathology. Gene Ontology (GO) pathways analysis revealed an over-representation of altered transcripts encoding proteins involved in oxidative phosphorylation (OXPHOS), specifically ATP synthesis, Ubiquinol to Cytochrome C and Cytochrome C to oxygen electron transport in the PN deregulated transcripts (Supplementary Table 3). As COQ8A is a mitochondrial protein, to further analyze the RNA sequencing data with a particular focus on mitochondrial pathways, we used mitoXplorer, an online tool for visualization and analysis of mitochondrial gene expression dynamics.[26] MitoXplorer revealed several deregulated pathways in PN involved in various mitochondrial functions. Similar to GO pathways analysis, OXPHOS was the most highly and significantly deregulated pathway in PN (Figure 3B and Supplementary Figure 2). In addition, transcripts from pathways such as translation, ROS defense and apoptosis were also overrepresented in the transcriptomic data of PN (Figure 3B). In contrast, no genes related to OXPHOS were significantly deregulated in GC (Figure 3B and Supplementary Table 3). We then further validated using RT-qPCR experiments that subunits from Complexes I-IV were downregulated in PN of *Coq8a*$^{-/-}$ mice (Figure 3C). Interestingly, at 5 weeks of age, one of the highest deregulated transcripts was *Cox6a2* (a subunit of the mitochondrial respiratory complex IV (COXIV)). As no specific antibodies against COX6a2 are available for western blot, the downregulation of COXIV was tested by immunostaining against another subunit of COXIV. This allowed us to confirm a significant decrease expression of COXIV in PN of 30 weeks old *Coq8a*$^{-/-}$ cerebellum compared to Ctrl animals (Figure 3D).

COQ8A deletion causes mitochondrial dysfunction and increased mitochondrial oxidative stress in PN

To investigate mitochondrial dysfunction upon COQ8A deletion, we performed histo-enzymatic reactions to quantify specifically in PNs the endogenous respiratory Complex I, II and IV activities from cerebellar slices of constitutive *Coq8a*$^{-/-}$ and Ctrl mice. All three respiratory complexes activities were found significantly decreased in PN of *Coq8a*$^{-/-}$ mice compared to Ctrl at 30 weeks of age (Figure 4A). To explore whether the activities of the respiratory complexes are altered at an earlier stage, we performed histo-enzymatic staining for the respiratory complexes II and IV at 5 weeks of age. In accordance with our LCM-RNA sequencing analysis that showed downregulation of Complex IV subunits (Figure 3C), the enzymatic activity of Complex IV was also found significantly decreased already at 5 weeks of age (Supplementary Figure 3B). However, Complex II activity showed no difference between *Coq8a*$^{-/-}$ and Ctrl mice, further suggesting that Complex IV is the first respiratory complex to be affected upon COQ8A deletion (Supplementary Figure 3A). Similarly, the activity of Complex IV was also found decreased in PNs of primary cultures at DIV21 (Supplementary Figure 3C). Quantitative spectroscopic measurement on whole cerebellum does not show any difference between the two genotypes (data not shown), probably as a result of the dilution effect of the rare Purkinje neurons (<1% cell population) compared to all the other abundant cell types. These results prompted us to further evaluate mitochondria respiration and fitness in the constitutive *Coq8a*$^{-/-}$ and Ctrl primary cerebellar cultures. To measure the mitochondrial membrane potential, we used live imaging with the potentiometric dye tetramethyl-rhodamine methyl ester (TMRM) in primary cultures at DIV21. PN from *Coq8a*$^{-/-}$ mice showed substantially decreased fluorescence intensity of TMRM compared to Ctrl PN, indicating aberrant mitochondrial membrane potential (Figure 4B). In addition, to evaluate the mitochondrial oxidative stress levels, we used the mitochondrial superoxide indicator MitoSOX^{TM} Red. Primary PN from *Coq8a*$^{-/-}$ mice had significantly increased fluorescence intensity of MitoSOX^{TM} Red, indicating elevated mitochondrial stress (Figure 4C). Altogether, these data demonstrate that constitutive COQ8A depletion in cerebellum leads to a mitochondrial dysfunction and increase mitochondrial oxidative stress specifically in PN.

COQ8A deletion causes Ca^{2+} concentration alterations in PN

Mitochondrial function and intracellular Ca^{2+} homeostasis are tightly linked, in particular mitochondria are important in clearing Ca^{2+} from synaptic terminals by their capacity to buffer

Ca^{2+} and to fuel Ca^{2+} clearance.[27–29] To evaluate if COQ8A deletion and the subsequent mitochondrial dysfunction would affect Ca^{2+} homeostasis in PN, we evaluated the expression levels of Ca^{2+} related proteins important for cerebellar function. Western blot and immunofluorescence experiments for Inositol 1,4,5-trisphosphate receptor type 1 (IP3R1), an endoplasmic reticulum (ER) Ca^{2+} channel highly expressed in cerebellar PN, was found more than two-fold decreased in the constitutive *Coq8a*$^{-/-}$ mice compared to controls (Figure 5A-B). Moreover, Western blot experiments on the conditional *Pcp2-Cre*;*Coq8a* $^{L+/L+}$ cerebellar extracts also showed decreased levels of IP3R1, suggesting that this decrease is specific to PN (Supplementary Figure 4). This decrease was not a consequence of PN death, as the PN-enriched ER calcium channel SERCA1 was not found to be deregulated in the constitutive *Coq8a*$^{-/-}$ mice (Figure 5C) nor calbindin (data not shown). To further explore Ca^{2+} homeostasis in cerebellum, we evaluated the phosphorylation of CAMKIIα, a calmodulin-depended kinase which upon increased intracellular Ca^{2+} levels auto-phosphorylates to become constitutively active.[30,31] Although CAMKIIα expression levels were not changed, the phosphorylated form was found significantly increased in cerebellar extract of the constitutive *Coq8a*$^{-/-}$ at 30 weeks of age, suggesting increased cytosolic Ca^{2+} levels (Figure 5D). Interestingly, electron microscopy analysis of the mitochondrial associated-ER membranes (MAMs), highly specialized subcellular compartments important for Ca^{2+} transport and signaling, were found to be dilated and fragmented in PN of constitutive *Coq8a*$^{-/-}$ animals (Figure 5E). To investigate at which time point the deregulation of calcium related proteins occurs, we performed IP3R1 western blot analysis on cerebellar lysates from constitutive *Coq8a*$^{-/-}$ and control mice at 5 and 10 weeks of age. Although at 5 weeks of age the IP3R1 protein levels were comparable between the two genotypes (Supplementary Figure 5A), at 10 weeks of age the level of expression was significantly decreased in the constitutive *Coq8a*$^{-/-}$ mice cerebellum (Supplementary Figure 5B). Finally, to validate the altered Ca^{2+} levels in *Coq8a*$^{-/-}$ PN, we performed live Ca^{2+} imaging using the next generation Ca^{2+} probe Calbryte™ 520 in primary cerebellar cultures derived from the constitutive *Coq8a*$^{-/-}$ and control mice at DIV21. Upon stimulation with 30mM KCl, *Coq8a*$^{-/-}$ PN exhibited more than 3-fold increased intracellular Ca^{2+} levels compared to the Ctrl PN (Figure 5F, Supplementary Figure 6). In contrast, the response of GCs on KCl stimulation showed no significant difference between the two genotypes (Figure 5G). Altogether, these results indicate altered intracellular Ca^{2+} concentration in *Coq8a*$^{-/-}$ PN, probably as a consequence of impaired mitochondrial calcium buffering.

Altered glutamate pathways in Coq8a$^{-/-}$ mice cerebellum

Glutamate neurotoxicity or alterations in its release and uptake are often reported in cerebellar ataxias.[32–34] Thus, we sought to determine the integrity of the glutamatergic synapses between PN and climbing fibers of the inferior olivary neurons using the presynaptic glutamate transporter vGLUT2. Immunofluorescence experiments revealed significantly decreased number of vGLUT2 puncta in the cerebellum of the constitutive *Coq8a*$^{-/-}$ mice at 30 weeks of age (Figure 6A, B). Moreover, the territory of the climbing fibers in molecular layer was found significantly decreased in *Coq8a*$^{-/-}$ mice (Figure 6C). vGLUT2 was also found significantly decreased by western blot analysis in *Coq8a*$^{-/-}$ mice cerebellum at 30 weeks of age (Figure 6D). In contrast, vGLUT1, the presynaptic glutamate transporters of the parallel fibers, showed no significant difference between *Coq8a*$^{-/-}$ and Ctrl mice (Figure 6D). Finally, vGAT, the presynaptic GABA transporter expressed in the presynaptic terminals of cerebellar interneurons, was also not found differentially expressed in *Coq8a*$^{-/-}$ cerebellar extracts (Fig 6D). To further investigate glutamate transport, we evaluated the expression levels of glutamate transporters in cerebellum. Although the expression of EAAT1, the glial glutamate transporter was not found altered, the expression levels of EAAT4, the PN-specific glutamate transporter, were found significantly downregulated in the constitutive *Coq8a*$^{-/-}$ mice cerebella (Figure 6E). To investigate at which time point the glutamate deregulation occurs in the *Coq8a*$^{-/-}$ mice cerebellum, we performed immunofluorescence and western blot analysis of vGLUT2 at the earlier disease stage of 5 and 10 weeks of age. Although at 5 weeks the expression levels of vGLUT2 were comparable between the two genotypes (Supplementary Figure 7C), at 10 weeks of age the vGLUT2 expression levels on western blot (Supplementary Figure 7B) as well as the number of vGLUT2 puncta on immunofluorescence analysis (Supplementary Figure 7A) were significantly decreased in the constitutive *Coq8a*$^{-/-}$ mice cerebellum compared to the control. Altogether, these data indicate that vGLUT2 signal is specifically decreased, with PN glutamate uptake being defective in *Coq8a*$^{-/-}$ mice cerebella. However, as no difference in vGLUT2 western blot or immunofluorescence signal was observed in the *Pcp2-Cre;Coq8a* $^{L+/L+}$ mice (Supplementary Figure 8A, B), this defect is therefore independent of COQ8A depletion in PN, and might be a consequence of COQ8A depletion in deep nuclei of the brainstem. This glutamate dysregulation could contribute to the more severe phenotype of the constitutive *Coq8a*$^{-/-}$ mice compared to the PN conditional mouse.

CoQ_{10} rescues PN cell number, morphology, mitochondria dysfunction and calcium intracellular levels in primary cerebellar cultures

Although CoQ_{10} deficiency was not observed in the cerebellum of *Coq8a*$^{-/-}$ mice[4] (probably due to the complexity of the tissues and signal dilution by unaffected granule cells), considering the primary role of COQ8A in regulating CoQ biosynthesis, we sought to determine if CoQ_{10} treatment could rescue the observed phenotype in PN. Primary cerebellar cultures treated with 10 μM of CoQ_{10} rescued the Coq8a$^{-/-}$ PN number (Figure 7A-B). Furthermore, *Coq8a*$^{-/-}$ PN treated with CoQ_{10} were indistinguishable in terms of morphology from Ctrl PN (Figure 7C-E). Moreover, CoQ_{10} treatment restored the mitochondrial membrane potential of *Coq8a*$^{-/-}$ PN to levels similar to Ctrl PN (Figure 7A,F). However, CoQ_{10} treatment only partially rescued the mitochondrial oxidative stress in *Coq8a*$^{-/-}$ PN (Figure 7A,G). Finally, CoQ_{10} treatment strongly decreased the intracellular levels of Ca^{2+} after KCl stimulation (Figure 7H,I). Together, these results give strong evidence that defects in PN are primarily linked to CoQ_{10} deficiency.

Discussion

In the current study, using complementary *in vivo* and *in vitro* experiments, we have uncovered the pivotal role of PN in the pathology of *COQ8A*-ataxia and the underlying molecular mechanism leading to PN-specific degeneration. In particular, we have shown that mitochondrial dysfunction in PN is an early pre-symptomatic event, leading consequently to increase mitochondrial oxidative stress, dysregulation of intracellular Ca^{2+} homeostasis and alteration in glutamate signaling. Furthermore, we have demonstrated that CoQ_{10} treatment *in vitro* rescues PN viability, morphology, mitochondrial function and Ca^{2+} buffering capacity.

Consistent to our previous observations, the laser microdissection enrichment approach showed that PN are primarily affected, with the number of deregulated transcripts in PN substantially higher than in GC. At the pre-symptomatic stage of 5 weeks, Gene ontology (GO) enrichment, mitoXplorer analysis point towards dysfunctional mitochondrial respiration, translation, ROS defense and apoptosis exclusively in PN. On the functional level, the mitochondrial dysfunction could be explained by COQ8A involvement in regulation of CoQ_{10} biosynthesis. Indeed, CoQ_{10} has an important role in the respiratory chain and acts as a potent

antioxidant. Surprisingly, despite a strong decrease in steady state levels of many components of the biosynthetic complex Q, no CoQ deficit could be detected in whole cerebellar extract .[4] However, we clearly demonstrated a decrease in mitochondrial function in PN, both *in vivo* and *in vitro*, with an increase in mitochondrial oxidative stress, which could be rescued *in vitro* by the addition of CoQ_{10} in the medium, further supporting that COQ8A deficiency most likely leads to CoQ deficit in PN. Conserning endogenous CoQ levels, we hypothesize that COQ8B activity in the other cerebellar cell population compensates COQ8A depletion. One question still pending is why, despite a strong deficit in the steady state levels of Complex Q components, no clear deficit in CoQ could be measured. While the enzymatic deficit in complex I, II and IV observed *in vivo* could be a direct consequence of oxidative stress, it is interesting to note that one of the transcripts that is most dysregulated in pre-symptomatic *Coq8a*$^{-/-}$ PN is Cox6a2, a subunit of Complex IV, as well as other transcript of Complex IV subunits. Interestingly, in a recent study, the COX6a1 subunit of complex IV was found to be a direct interactor of COQ8A in HEK293 and HepG2 human cell lines,[35] suggesting that COQ8A could directly interact with a subunit of the respiratory complex IV. Could the downregulation of *Cox6a2*, an important isoform of Cox6a1 found in Pvalb+ neurons important for regulating ATP synthesis since it is able to adjust the catalytic activity of Complex IV, be an indirect consequence of this interaction with COQ8A? Interestingly, *Cox6a2* depleted mice have been reported to show decreased enzymatic Complex IV activity and increased ROS production.[36]

Purkinje neurons are probably the neurons with the highest metabolic activity in the central nervous system.[37] They receive hundreds of thousands of glutamatergic synapses and in order to tightly maintain Ca^{2+} homeostasis, they express a variety of Ca^{2+} channels, Ca^{2+}-dependent kinases, phosphatases, and Ca^{2+}-binding proteins.[38,39] Defective mitochondrial function in PN is followed by inefficient mitochondrial calcium buffering.[15,40] Thus, the interplay between proper mitochondrial respiration and Ca^{2+} handling is extremely important for the proper function of PN. Conversely, mutations on Ca^{2+} channels, glutamate receptors and mitochondria proteins are often associated with PN dysfunction and ataxia.[38,41–43] In this study, we showed for the first time that *Coq8a*$^{-/-}$ PN are characterized by dysregulated Ca^{2+} homeostasis, with decreased expression levels of IP3R1. There are 3 known allosteric modulators of IP3R1: IP3, Ca^{2+} and ATP.[44] Although little is known about the regulation of IP3R1 by ATP, increased activation of glutamatergic synapses and IP3 release, as well as increased intracellular [Ca^{2+}] negatively regulate IP3R1 expression, thus protecting neurons from toxic levels of Ca^{2+}, by

desensitizing endoplasmic reticulum to Ca^{2+} release.[42,44–46] Interestingly, the dark cell degeneration, such as observed in *Coq8a*$^{-/-}$ PN,[4] has also been shown to occur under mitochondrial dysfunction and the subsequent Ca^{2+} deregulation in a mouse model of SCA28.[15,47] Furthermore, the downregulations of glutamate transporters such as vGLUT2 and EAAT4 may indicate that glutamate might not be properly recycled in PN synapses. The latter event could also contribute to increased Ca^{2+} influx and IP3 release in PN, further negatively regulating IP3R1. Although beyond this study, these results point out to the possibility of using Ceftriaxone as a treatment strategy for COQ8A-ataxia. Indeed, recently, Ceftriaxone, by increasing the expression of EAAT2 glutamate transporters, has been shown to be one of the most promising compounds for the reduction of glutamate excitotoxicity, the restoration of intracellular Ca^{2+} levels and ultimately the alleviation of motor deficits in mouse models of ataxias and other neurodegenerative disorders.[15,48,49]

While in other ataxias, the decreased IP3R1 expression levels was due to direct interaction between the poly-Q mutated proteins and IP3R1,[13,38] in *Coq8a*$^{-/-}$ mice it remains unknown why IP3R1 was found downregulated. An explanation could involve an allosteric regulation of IP3R1 stability and activity through elevated Ca^{2+} levels. Although little is known about the regulation of IP3R1 by Ca^{2+}, it has been shown that excessive binding of Ca^{2+} in the regulatory domain of IP3R1 reduced its activity while simultaneously increased its recycling.[42,44,45,50] Thus, the observed downregulation of IP3R1 could act as a protective mechanism against further Ca^{2+} release from the ER, reducing the toxic consequences for the cell. IP3R1 is also known as an indispensable component of the Mitochondrial Associated Membranes (MAMs), the lipid rafts between ER and mitochondria.[27,28,51] Ca^{2+} but also other molecules such as cholesterol and CoQ_{10} precursors are transferred from ER to mitochondria.[27,51,52] Recent published results demonstrated that Complex Q is localizing in MAMs being part of the mitochondrial side of MAMs.[53] The functional hypothesis is that Complex Q localizes in a substrate dependent manner at the ER–mitochondria contact sites, to promote access to CoQ lipid intermediates coming from ER, for efficient CoQ production and distribution.[53,54] Noteworthy, our ultrastructural analysis of *Coq8a*$^{-/-}$ PN indicated that mitochondrial associated membranes had altered structures presenting enlarged – swollen spaces between the two organelles.

Primary CoQ deficiencies are characterized by a various range of tissue specificities and clinical severities, for yet unknown reasons.[9] Variable expression of COQ proteins could reflect the increased tissue susceptibility of a primary CoQ deficiency over another. In this study, the

differential expression of COQ8A and COQ8B in cerebellum provide a molecular explanation for the specific PN dysfunction observed in the *Coq8a*$^{-/-}$ mouse model and thus the cerebellar ataxia in patients. The remarkably low levels of COQ8B expression in PN in addition to the high levels of COQ8A expression, could possibly explain the vulnerability of these neurons upon COQ8A deletion. The transcriptomic data further support that COQ8B could compensate for COQ8A loss in GC. The generation of *Pcp2-Cre;Coq8a*$^{L+/L+}$ mouse model and its resulting ataxic phenotype further solidifies the central role of PN in COQ8A-ataxia pathology. However, *Pcp2-Cre;Coq8a*$^{L+/L+}$ mice motor dysfunction started at the age of 15-20 weeks, a timepoint slightly delayed compared to the constitutive *Coq8a*$^{-/-}$ mice which starts at 10 weeks,[4] and showed no dysregulation of vGLUT2. These data suggest that deletion of COQ8A in the other cells of the central nervous system (deep nuclei of brain stem), and/or the muscles, or at earlier during embryogenesis contribute to the motor phenotype in the constitutive knockout.

Due to its antioxidant function, CoQ_{10} and its analogs such as Mito-Q have been used for therapy in a variety of neurodegenerative disorders ranging from ataxias such as SCA1 to Parkinson's disease and amyotrophic lateral sclerosis.[20,55–57] In contrast to the later neurodegenerative disorders, treatment with CoQ_{10} in CoQ_{10}-defiencies targets the primary source of the pathology and not just to reduce the load of the toxic free radicals. Up to date, promising results are coming from studies reporting that CoQ_{10} supplementation can stop the progression of the encephalopathy, ataxia and nephrotic syndromes in patients with CoQ_{10} deficiencies.[11,58–61] In the largest study up to date, 30 COQ8A-ataxia patients with various COQ8A mutations were treated with CoQ_{10} using a mean cumulative daily dose of 11 mg/kg/day.[3] Based on the clinical reports, 13/30 patients responded positively and 15/30 did not. Qualitative measurements of the treatment follow up showed improvement of ataxia, but also of tremor, dystonia, epilepsy, mental speed and muscle weakness.[3] The relatively high number of non-responders could be explained by the poor biodistribution of pure CoQ_{10} in the CNS. In the present study, we demonstrated for the first time that direct application of 10 µM of CoQ_{10} on primary cerebellar cultures almost completely reverses the morphological and mitochondrial phenotype of *Coq8a*$^{-/-}$ PN. Furthermore, CoQ_{10} completely rescued the mitochondrial membrane potential, and reduced the oxidative stress inside mitochondria. In addition, CoQ_{10} application improved Ca^{2+} handling after KCl stimulation of *Coq8a*$^{-/-}$ PN. These results suggest that the Ca^{2+} deficiency in COQ8A-depleted mouse PN is a consequence of the mitochondrial dysfunction probably due to CoQ_{10} reduction. Beyond the current

manuscript, our results suggests that blood brain barrier penetrant CoQ_{10} analogs could be very beneficial treatments for COQ8A-ataxia patients and should therefore be tested in preclinical animal models.

Acknowledgements

We thank Nadia Messaddeq from the IGBMC imaging platform for EM analysis. We thank the members of the Puccio laboratory for critical reading of the manuscript.

Funding

This work was supported by ANR-15-RAR3-0011 under the frame of the E-Rare-3 network PREPARE, TREATARCA and FRM (to HP). This study was supported by the grant ANR-10-LABX-0030-INRT, a French State fund managed by the Agence Nationale de la Recherche under the frame program Investissement d'Avenir ANR-10-IDEX-0002-02.

Competing interests

The authors report no competing interests.

Supplementary material

Supplementary material is available at *Brain* online.

References

1. Lagier-Tourenne C, Tazir M, López LC, et al. ADCK3, an Ancestral Kinase, Is Mutated in a Form of Recessive Ataxia Associated with Coenzyme Q10 Deficiency. *Am J Hum Genet*. 2008;82(3):661-672. doi:10.1016/j.ajhg.2007.12.024
2. Mollet J, Delahodde A, Serre V, et al. CABC1 Gene Mutations Cause Ubiquinone Deficiency with Cerebellar Ataxia and Seizures. *Am J Hum Genet*. 2008;82(3):623-630. doi:10.1016/j.ajhg.2007.12.022
3. Traschütz A, Schirinzi T, Laugwitz L, et al. Clinico-genetic, imaging and molecular

delineation of COQ8A -ataxia: a multicenter study of 59 patients . *Ann Neurol*. April 2020. doi:10.1002/ana.25751

4. Stefely JA, Licitra F, Laredj L, et al. Cerebellar Ataxia and Coenzyme Q Deficiency through Loss of Unorthodox Kinase Activity. *Mol Cell*. 2016;63(4):608-620. doi:10.1016/j.molcel.2016.06.030

5. Reidenbach AG, Kemmerer ZA, Aydin D, et al. Conserved Lipid and Small-Molecule Modulation of COQ8 Reveals Regulation of the Ancient Kinase-like UbiB Family. *Cell Chem Biol*. 2017:1-12. doi:10.1016/j.chembiol.2017.11.001

6. Stefely JA, Reidenbach AG, Ulbrich A, et al. Mitochondrial ADCK3 employs an atypical protein kinase-like fold to enable coenzyme Q Biosynthesis. *Mol Cell*. 2015;57(1):83-94. doi:10.1016/j.molcel.2014.11.002

7. Xie LX, Hsieh EJ, Watanabe S, et al. Expression of the human atypical kinase ADCK3 rescues coenzyme Q biosynthesis and phosphorylation of Coq polypeptides in yeast coq8 mutants. *Biochim Biophys Acta - Mol Cell Biol Lipids*. 2011;1811(5):348-360. doi:10.1016/j.bbalip.2011.01.009

8. Cullen JK, Abdul Murad N, Yeo A, et al. Correction: AarF Domain Containing Kinase 3 (ADCK3) mutant cells display signs of oxidative stress, defects in mitochondrial homeostasis and lysosomal accumulation. *PLoS One*. 2016;11(7):1-28. doi:10.1371/journal.pone.0160162

9. Laredj LN, Licitra F, Puccio HM. The molecular genetics of coenzyme Q biosynthesis in health and disease. *Biochimie*. 2014;100(1):78-87. doi:10.1016/j.biochi.2013.12.006

10. Acosta MJ, Vazquez Fonseca L, Desbats MA, et al. Coenzyme Q biosynthesis in health and disease. *Biochim Biophys Acta - Bioenerg*. 2016;1857(8):1079-1085. doi:10.1016/j.bbabio.2016.03.036

11. Ashraf S, Gee HY, Woerner S, et al. ADCK4 mutations promote steroid-Resistant nephrotic syndrome through CoQ10 biosynthesis disruption. *J Clin Invest*. 2013;123(12):5179-5189. doi:10.1172/JCI69000

12. Widmeier E, Yu S, Nag A, et al. ADCK4 Deficiency Destabilizes the Coenzyme Q Complex, Which Is Rescued by 2,4-Dihydroxybenzoic Acid Treatment. *J Am Soc Nephrol*. 2020;31(6):1191-1211. doi:10.1681/ASN.2019070756

13. Kasumu A, Bezprozvanny I. Deranged calcium signaling in purkinje cells and

pathogenesis in spinocerebellar ataxia 2 (SCA2) and other ataxias. *Cerebellum*. 2012;11(3):630-639. doi:10.1007/s12311-010-0182-9

14. Strahlendorf JC, Acosta S, Strahlendorf HK. Diazoxide and cyclothiazide convert AMPA-induced dark cell degeneration of Purkinje cells to edematous damage in the cerebellar slice. *Brain Res*. 1996;729(2):197-204. doi:10.1016/0006-8993(96)00367-8

15. Maltecca F, Baseggio E, Consolato F, et al. Purkinje neuron Ca2+ influx reduction rescues ataxia in SCA28 model. *J Clin Invest*. 2015;125(1):263-274. doi:10.1172/JCI74770

16. Simon D. Friedreich Ataxia Mouse Models with Progressive Cerebellar and Sensory Ataxia Reveal Autophagic Neurodegeneration in Dorsal Root Ganglia. *J Neurosci*. 2004;24(8):1987-1995. doi:10.1523/JNEUROSCI.4549-03.2004

17. Tabata T, Sawada S, Araki K, Bono Y, Furuya S, Kano M. A reliable method for culture of dissociated mouse cerebellar cells enriched for Purkinje neurons. *J Neurosci Methods*. 2000;104(1):45-53. doi:10.1016/S0165-0270(00)00323-X

18. Stoyas CA, Bushart DD, Switonski PM, et al. Nicotinamide Pathway-Dependent Sirt1 Activation Restores Calcium Homeostasis to Achieve Neuroprotection in Spinocerebellar Ataxia Type 7. *Neuron*. 2020;105(4):630-644.e9. doi:10.1016/j.neuron.2019.11.019

19. Perkins EM, Clarkson YL, Suminaite D, et al. Loss of cerebellar glutamate transporters EAAT4 and GLAST differentially affects the spontaneous firing pattern and survival of Purkinje cells. *Hum Mol Genet*. 2018;27(15):2614. doi:10.1093/hmg/ddy169

20. Stucki DM, Ruegsegger C, Steiner S, et al. Mitochondrial impairments contribute to Spinocerebellar ataxia type 1 progression and can be ameliorated by the mitochondria-targeted antioxidant MitoQ. *Free Radic Biol Med*. 2016;97:427-440. doi:10.1016/j.freeradbiomed.2016.07.005

21. Martin M. Cutadapt removes adapter sequences from high-throughput sequencing reads. *EMBnet.journal*. 2011;17(1):10. doi:10.14806/ej.17.1.200

22. Langmead B, Salzberg SL. Fast gapped-read alignment with Bowtie 2. *Nat Methods*. 2012;9(4):357-359. doi:10.1038/nmeth.1923

23. Dobin A, Davis CA, Schlesinger F, et al. STAR: Ultrafast universal RNA-seq aligner. *Bioinformatics*. 2013;29(1):15-21. doi:10.1093/bioinformatics/bts635

24. Anders S, Pyl PT, Huber W. HTSeq-A Python framework to work with high-throughput sequencing data. *Bioinformatics*. 2015;31(2):166-169. doi:10.1093/bioinformatics/btu638

25. Love MI, Huber W, Anders S. Moderated estimation of fold change and dispersion for RNA-seq data with DESeq2. *Genome Biol*. 2014;15(12). doi:10.1186/s13059-014-0550-8

26. Yim A, Koti P, Bonnard A, et al. MitoXplorer, a visual data mining platform to systematically analyze and visualize mitochondrial expression dynamics and mutations. *Nucleic Acids Res*. 2020;48(2):605-632. doi:10.1093/nar/gkz1128

27. Santo-Domingo J, Demaurex N. Calcium uptake mechanisms of mitochondria. *Biochim Biophys Acta - Bioenerg*. 2010;1797(6-7):907-912. doi:10.1016/j.bbabio.2010.01.005

28. Rizzuto R, De Stefani D, Raffaello A, Mammucari C. Mitochondria as sensors and regulators of calcium signalling. *Nat Rev Mol Cell Biol*. 2012;13(9):566-578. doi:10.1038/nrm3412

29. Lee KS, Huh S, Lee S, et al. Erratum: Altered ER-mitochondria contact impacts mitochondria calcium homeostasis and contributes to neurodegeneration in vivo in disease models (Proceedings of the National Academy of Sciences of the United States of America (2018) 115 (E8844-E8853) DOI: *Proc Natl Acad Sci U S A*. 2018;115(42):E9992. doi:10.1073/pnas.1815900115

30. Miller SG, Kennedy MB. Regulation of brain type II Ca2+/calmodulin-dependent protein kinase by autophosphorylation: a Ca2+-triggered molecular switch. *Cell*. 1986;44(6):861-870. doi:10.1016/0092-8674(86)90008-5

31. Swulius MT, Waxham MN. Ca2+/calmodulin-dependent protein kinases. *Cell Mol Life Sci*. 2008;65(17):2637-2657. doi:10.1007/s00018-008-8086-2

32. Hoxha E, Balbo I, Mc M, Tempia F. Purkinje Cell Signaling Deficits in Animal Models of Ataxia. *Purkinje Cell Signal Deficits Anim Model Ataxia Front Synaptic Neurosci*. 2018;10:6. doi:10.3389/fnsyn.2018.00006

33. Hirai H, Kano M. Type 1 metabotropic glutamate receptor and its signaling molecules as therapeutic targets for the treatment of cerebellar disorders. *Curr Opin Pharmacol*. 2018;38:51-58. doi:10.1016/j.coph.2018.02.002

34. Meera P, Pulst SM, Otis TS. Cellular and circuit mechanisms underlying spinocerebellar

ataxias. *J Physiol*. 2016;594(16):4653-4660. doi:10.1113/JP271897

35. Floyd BJ, Wilkerson EM, Veling MT, et al. Mitochondrial Protein Interaction Mapping Identifies Regulators of Respiratory Chain Function. *Mol Cell*. 2016;63(4):621-632. doi:10.1016/j.molcel.2016.06.033

36. Quintens R, Singh S, Lemaire K, et al. Mice Deficient in the Respiratory Chain Gene Cox6a2 Are Protected against High-Fat Diet-Induced Obesity and Insulin Resistance. *PLoS One*. 2013;8(2). doi:10.1371/journal.pone.0056719

37. Kitamura K, Kano M. Dendritic calcium signaling in cerebellar Purkinje cell. *Neural Networks*. 2013;47:11-17. doi:10.1016/j.neunet.2012.08.001

38. Prestori F, Moccia F, D'angelo E. Disrupted calcium signaling in animal models of human spinocerebellar ataxia (SCA). *Int J Mol Sci*. 2020;21(1). doi:10.3390/ijms21010216

39. Smeets CJLM, Verbeek DS. Neurobiology of Disease Climbing fi bers in spinocerebellar ataxia : A mechanism for the loss of motor control. *Neurobiol Dis*. 2016;88:96-106. doi:10.1016/j.nbd.2016.01.009

40. Patron M, Sprenger HG, Langer T. M-AAA proteases, mitochondrial calcium homeostasis and neurodegeneration. *Cell Res*. 2018;28(3):296-306. doi:10.1038/cr.2018.17

41. Synofzik M, Puccio H, Mochel F, Schöls L. Autosomal Recessive Cerebellar Ataxias: Paving the Way toward Targeted Molecular Therapies. *Neuron*. 2019;101(4):560-583. doi:10.1016/j.neuron.2019.01.049

42. Hisatsune C, Hamada K, Mikoshiba K. Ca2+ signaling and spinocerebellar ataxia. *Biochim Biophys Acta - Mol Cell Res*. 2018;1865(11):1733-1744. doi:10.1016/J.BBAMCR.2018.05.009

43. Shimobayashi E, Kapfhammer JP. Calcium Signaling, PKC Gamma, IP3R1 and CAR8 Link Spinocerebellar Ataxias and Purkinje Cell Dendritic Development. *Curr Neuropharmacol*. 2018;16(2):151-159. doi:10.2174/1570159X15666170529104000

44. Egorova PA, Bezprozvanny IB. Inositol 1,4,5-trisphosphate receptors and neurodegenerative disorders. *FEBS J*. January 2018. doi:10.1111/febs.14366

45. Wojcikiewicz RJH. The Making and Breaking of Inositol 1,4,5-Trisphosphate Receptor

Tetramers. *Messenger*. 2019;6(1):45-49. doi:10.1166/msr.2018.1073

46. Wright FA, Wojcikiewicz RJH. *Chapter 4 - Inositol 1,4,5-Trisphosphate Receptor Ubiquitination*. Vol 141. Elsevier Inc.; 2016. doi:10.1016/bs.pmbts.2016.02.004

47. Maltecca F, Magnoni R, Cerri F, Cox GA, Quattrini A, Casari G. Haploinsufficiency of AFG3L2, the Gene Responsible for Spinocerebellar Ataxia Type 28, Causes Mitochondria-Mediated Purkinje Cell Dark Degeneration. *J Neurosci*. 2009;29(29):9244-9254. doi:10.1523/JNEUROSCI.1532-09.2009

48. Rothstein JD, Patel S, Regan MR, et al. β-Lactam antibiotics offer neuroprotection by increasing glutamate transporter expression. *Nature*. 2005;433(7021):73-77. doi:10.1038/nature03180

49. Leung TCH, Lui CNP, Chen LW, Yung WH, Chan YS, Yung KKL. Ceftriaxone ameliorates motor deficits and protects dopaminergic neurons in 6-hydroxydopamine-lesioned rats. *ACS Chem Neurosci*. 2012;3(1):22-30. doi:10.1021/cn200072h

50. Hattori M, Mikoshiba K, Hashikawa T, et al. Type 1 Inositol Trisphosphate Receptor Regulates Cerebellar Circuits by Maintaining the Spine Morphology of Purkinje Cells in Adult Mice. *J Neurosci*. 2013;33(30):12186-12196. doi:10.1523/jneurosci.0545-13.2013

51. Rizzuto R, Pinton P, Carrington W, et al. Close contacts with the endoplasmic reticulum as determinants of mitochondrial Ca2+ responses. *Science (80-)*. 1998;280(5370):1763-1766. doi:10.1126/science.280.5370.1763

52. Vid V, Günther D. Lipid Transport between the Endoplasmic Reticulum and Mitochondria. *Cold Spring Harb Perspect Biol*. 2013;5:0. doi:10.1101/cshperspect.a013391

53. Subramanian K, Jochem A, Vasseur M Le, et al. Coenzyme Q biosynthetic proteins assemble in a substrate-dependent manner into domains at ER-mitochondria contacts. *J Cell Biol*. 2019;218(4):1352-1368. doi:10.1083/jcb.201808044v

54. Kemmerer ZA, Robinson KP, Schmitz JM, et al. UbiB proteins regulate cellular CoQ distribution in Saccharomyces cerevisiae. *Nat Commun*. 2021;12(1):1-11. doi:10.1038/s41467-021-25084-7

55. Miquel E, Cassina A, Martínez-Palma L, et al. Neuroprotective effects of the mitochondria-targeted antioxidant MitoQ in a model of inherited amyotrophic lateral

sclerosis. *Free Radic Biol Med*. 2014;70:204-213. doi:10.1016/j.freeradbiomed.2014.02.019

56. Ghosh A, Chandran K, Kalivendi S V., et al. Neuroprotection by a mitochondria-targeted drug in a Parkinson's disease model. *Free Radic Biol Med*. 2010;49(11):1674-1684. doi:10.1016/j.freeradbiomed.2010.08.028

57. Rodriguez-Cuenca S, Cochemé HM, Logan A, et al. Consequences of long-term oral administration of the mitochondria-targeted antioxidant MitoQ to wild-type mice. *Free Radic Biol Med*. 2010;48(1):161-172. doi:10.1016/j.freeradbiomed.2009.10.039

58. Salviati L, Sacconi S, Murer L, et al. Infantile encephalomyopathy and nephropathy with CoQ10 deficiency: a CoQ10-responsive condition. *Neurology*. 2005;65(4):606-608. doi:10.1212/01.wnl.0000172859.55579.a7

59. Quinzii C, Naini A, Salviati L, Trevisson E, Dimauro S, Hirano M. Report A Mutation in Para-Hydroxybenzoate-Polyprenyl Transferase (COQ2) Causes Primary Coenzyme Q 10 Deficiency. *Am J Hum Genet*. 2006;78:345-349.

60. Atmaca M, Gulhan B, Korkmaz E, et al. Follow-up results of patients with ADCK4 mutations and the efficacy of CoQ10 treatment. *Pediatr Nephrol*. 2017;32(8):1369-1375. doi:10.1007/s00467-017-3634-3

61. Atmaca M, Gülhan B, Atayar E, et al. Long-term follow-up results of patients with ADCK4 mutations who have been diagnosed in the asymptomatic period: effects of early initiation of CoQ10 supplementation. *Turk J Pediatr*. 2019;61(5):657-663. doi:10.24953/turkjped.2019.05.003

Figure legends

Figure 1 COQ8A expression pattern in the cerebellum. Representative images of immunofluorescence on sagittal cerebellar slices from control (Ctrl) and Coq8a$^{-/-}$ mice at 30 weeks of age for COQ8A (**A**), COQ7 (**B**), COQ5 (**C**) COQ8B (**D**). Scale bar = 25µm E) Western blot analysis on cerebellar extracts from control (Ctrl) and Coq8a$^{-/-}$ mice at 30 weeks of age. GAPDH is used as a loading control.

Figure 2 *Coq8a* deletion in PN causes ataxia and alters their morphology. **(A)** Accerelating rotarod retention time from 10 weeks until 25 weeks in *PCP2-Cre;Coq8a* $^{L+/L+}$ and Ctrl animals (females n=12, mean ± SEM, and males n=12, mean ± SEM, 2-way ANOVA, **p-value<0.01, *p-value<0.05. (**B**) Footprint analysis. Linearity which is proportional to non-linear movement and miss-matching of hind and front paws overlap, (n=12, mean ± SEM, Student t test, ***p-value<0.001, **p-value<0.01, *p-value<0.05). (**C**) Immunofluorescence using CALB1 antibody on sagittal cerebellar slices of Ctrl and *PCP2-Cre;Coq8a* $^{L+/L+}$ mice at 30 weeks of age. White asterisks point to absent PN. Scale bar= 25µm (**D**) Immunofluorescence using CALB1 antibody on DIV21 primary cerebellar cultures derived from P0 Ctrl and *Coq8a*$^{-/-}$ pups. Scale bar= 25µm Quantification of number of PN neurons in the cultures expressed as a percentage of total cells (n>80 PN, 6 biological replicates, mean ± SEM, Student t test ****p-value<0.0001). (**E**) Representative image of control PN stained with CALB1 antibody. Morphological analysis of PN complexity. Primary nodes (white asterisks) and width of PN dendrites, as well as PN area covered were measured and compared between Ctrl and *Coq8a*$^{-/-}$ mice, (n> 30 PN, 6 biological replicates).

Figure 3 RNA-sequencing after LCM in PN and GC. (**A**) Venn diagram for the comparison of significantly deregulated transcripts after RNA-Sequencing of Laser Capture Microdissection (LCM) of PN and GC from Ctrl and *Coq8a*$^{-/-}$ mice (n=6) at the pre-symptomatic stage of 5 weeks of age. (**B**) Graphical illustration of the deregulated genes found in PN and GC of *Coq8a*$^{-/-}$ mice, grouped in 35 mitochondrial pathways using mitoXplorer tool. Red or blue color represents respectively down- or up-regulation of the transcripts and the size of the circle shows the fold change of the transcripts. (**C**) RT-qPCR validation of the deregulated transcripts involved in ATP synthesis. n=6, mean ± SEM, Student t test, ***p-value<0.001. (**D**) Immunofluorescence using COXIV antibody and quantification of fluorescence intensity in PN from cerebellar slices at 30 weeks of age. PN are highlighted in white. Scale bar= 25µm

Figure 4 Mitochondrial deficiency in Coq8a$^{-/-}$ mice. (A) Complex I, SDH and COXIV histo-enzymatic staining using sagittal sections of cerebellum from Ctrl and Coq8a$^{-/-}$ mice at 30 weeks of age. PN are highlighted in red (n>50 PN, 6 biological replicates, Student t test, ****p-value<0.0001, Scale bars = 25 mm). (**B**) Live imaging using TMRM probe in primary cerebellar cultures at DIV21 (n>50 PN, 6 biological replicates, Student t test, ***p-value<0.001, Scale bars = 25 mm). (**C**) Live imaging using MitoSOX in primary cerebellar

cultures at DIV21 (n>25 PN, 6 biological replicates, mean ± SEM , Student t test, ****p-values<0.0001, Scale bars = 25 mm).

Figure 5 Altered expression of Ca^{2+} channels and Ca^{2+} homeostasis in Coq8a$^{-/-}$ mice. (**A**) Double immunofluorescence using CALB1 and IP3R1 antibodies in Ctrl and Coq8a$^{-/-}$ cerebellum from mice at 30 weeks of age (Scale bars = 25 mm). (**B,C,D**) Western blot for IP3R1, SERCA1 and p-CAMKIIα (n=6, mean ± SEM , Student t test,**p-value <0.01). E) Electron microscopy from Ctrl and *Coq8a*$^{-/-}$PN at 30 weeks of age (Scale bars = 2 mm). Arrows indicate swollen contacts sites between mitochondrial and ER. (**F,G**) Live calcium imaging using the single wavelength probe Calbryte520TM on KCl stimulated primary cerebellar cultures at DIV21. (n>25 PNs or GCs, 6 biological replicates, mean ± SEM, Student t test, ****p-value<0.0001).

Figure 6 COQ8A deletion alters the expression of glutamate transporters. (**A**) Double immunofluorescence using CALB1 and vGLUT2 antibodies in Ctrl and *Coq8a*$^{-/-}$ cerebellum from mice at 30 weeks of age (Scale bars = 25 mm). (**B**) Number of vGLUT2 synapses in the molecular layer (ML) of Ctrl and *Coq8a*$^{-/-}$ mice (n=6, mean ± SEM, Student t test, *p-value<0.05). (**C**) Measurement of the ratio between the length of vGLUT2 territory and the total ML length (n=6, mean ± SEM, Student t test, *p-value< 0.05). (**D**) Western blot experiments and quantifications for vGLUT2, vGLUT1 and vGAT, respectively (n=6, mean ± SEM, Student t test, *p-value< 0.05). (**E**) Western blots for EAAT1 and EAAT4 and their quantification (n=6, mean ± SEM, Student t test, **p-value < 0.01).

Figure 7 Rescue of primary PN using CoQ10. (**A-E**) Immunofluorescence using CALB1 antibody in Ctrl, *Coq8a*$^{-/-}$ and *Coq8a*$^{-/-}$ treated with CoQ_{10} primary cultures at DIV21 (Scale bar = 25 mm). Effect of 10 µm CoQ_{10} treatment on the number and morphology of *Coq8a*$^{-/-}$ PN(n>80 PN, 6 biological replicates, Student t test, ****p-value<0.0001). (**A,F**) Effect of 10 µm CoQ_{10} treatment on the mitochondrial membrane potential as indicated by TMRM intensity (n>50 PN, 6 biological replicates, Student t test, ***p-value<0.001). (**A,G**) CoQ_{10} treatment reduces oxidative stress in *Coq8a*$^{-/-}$ PN as indicated by MitoSOX intensity (n>25 PN, 6 biological replicates, Student t test, *p-value<0.05, ****p-value<0.001). (**H,I**) Effect of CoQ10 treatment on the intracellular calcium levels as indicated by Calbryte 520^{TM}. after stimulation by KCl at DIV21. (n>25 PN, 6 biological replicates, mean ± SEM, Student t test, ****p-value<0.0001).

Figure 1

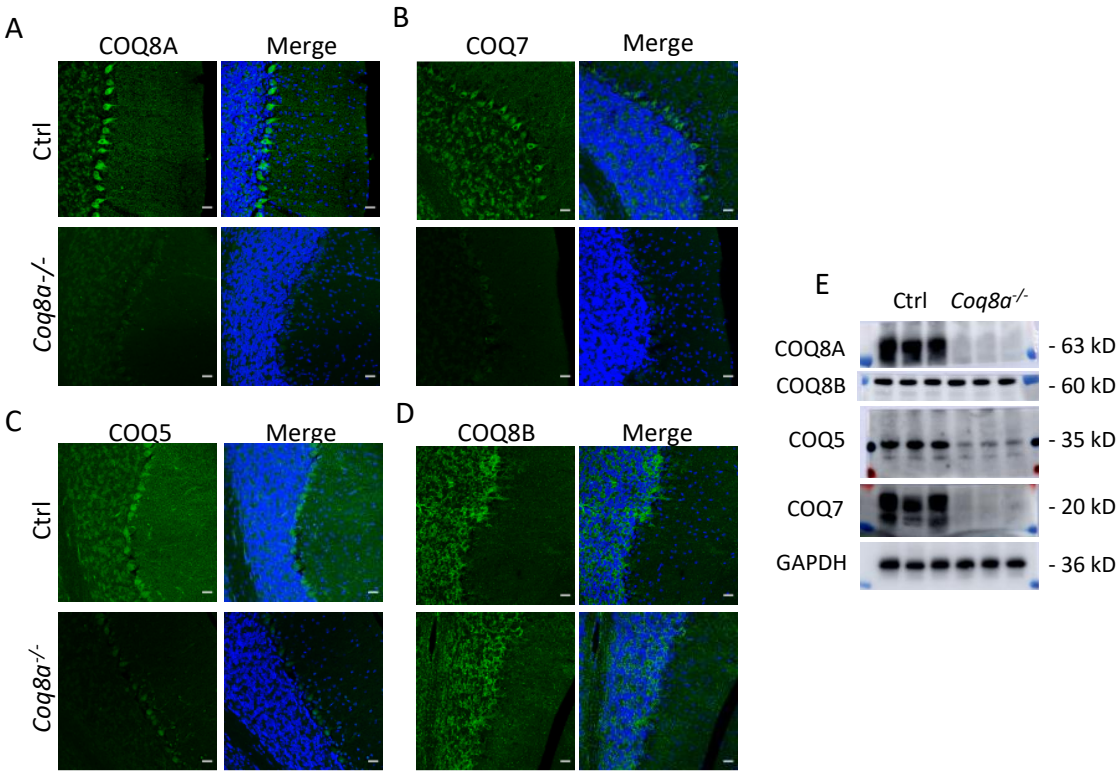
A
COQ8A
Merge
Ctrl
Coq8a-/-
B
COQ7
Merge
C
COQ5
Merge
Ctrl
Coq8a-/-
D
COQ8B
Merge
E
Ctrl
Coq8a-/-
COQ8A
- 63 kD
COQ8B
- 60 kD
COQ5
- 35 kD
COQ7
- 20 kD
GAPDH
- 36 kD

Figure 2

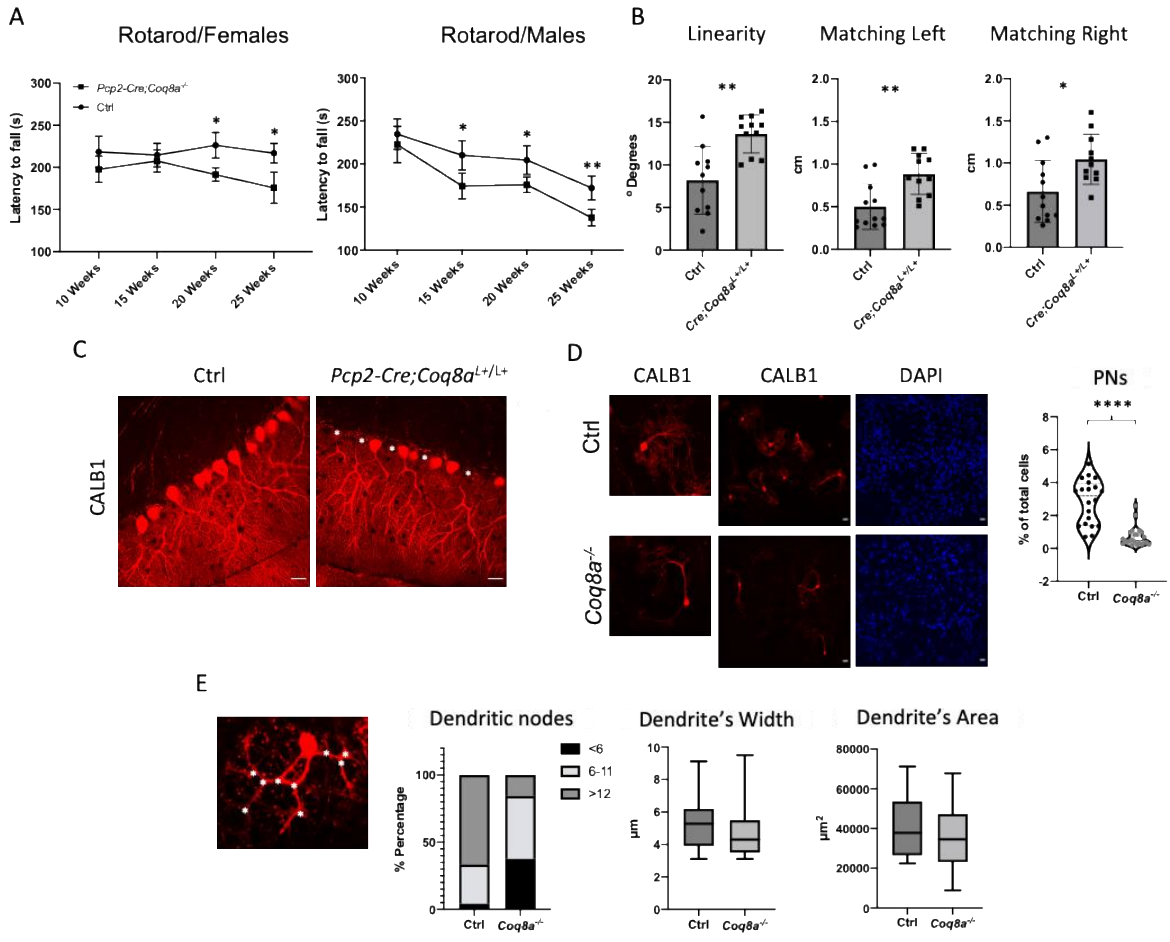
A
Rotarod/Females
Rotarod/Males
Latency to fall (s)
Pcp2-Cre;Coq8a-/-
Ctrl
10 Weeks
15 Weeks
20 Weeks
25 Weeks
B
Linearity
Matching Left
Matching Right
° Degrees
cm
Ctrl
Cre;Coq8aL+/L+
C
Ctrl
Pcp2-Cre;Coq8aL+/L+
CALB1
D
CALB1
CALB1
DAPI
Ctrl
Coq8a-/-
PNs
% of total cells
E
Dendritic nodes
Dendrite's Width
Dendrite's Area
% Percentage
<6
6-11
>12
µm
µm2
Coq8a-/-

Figure 3.

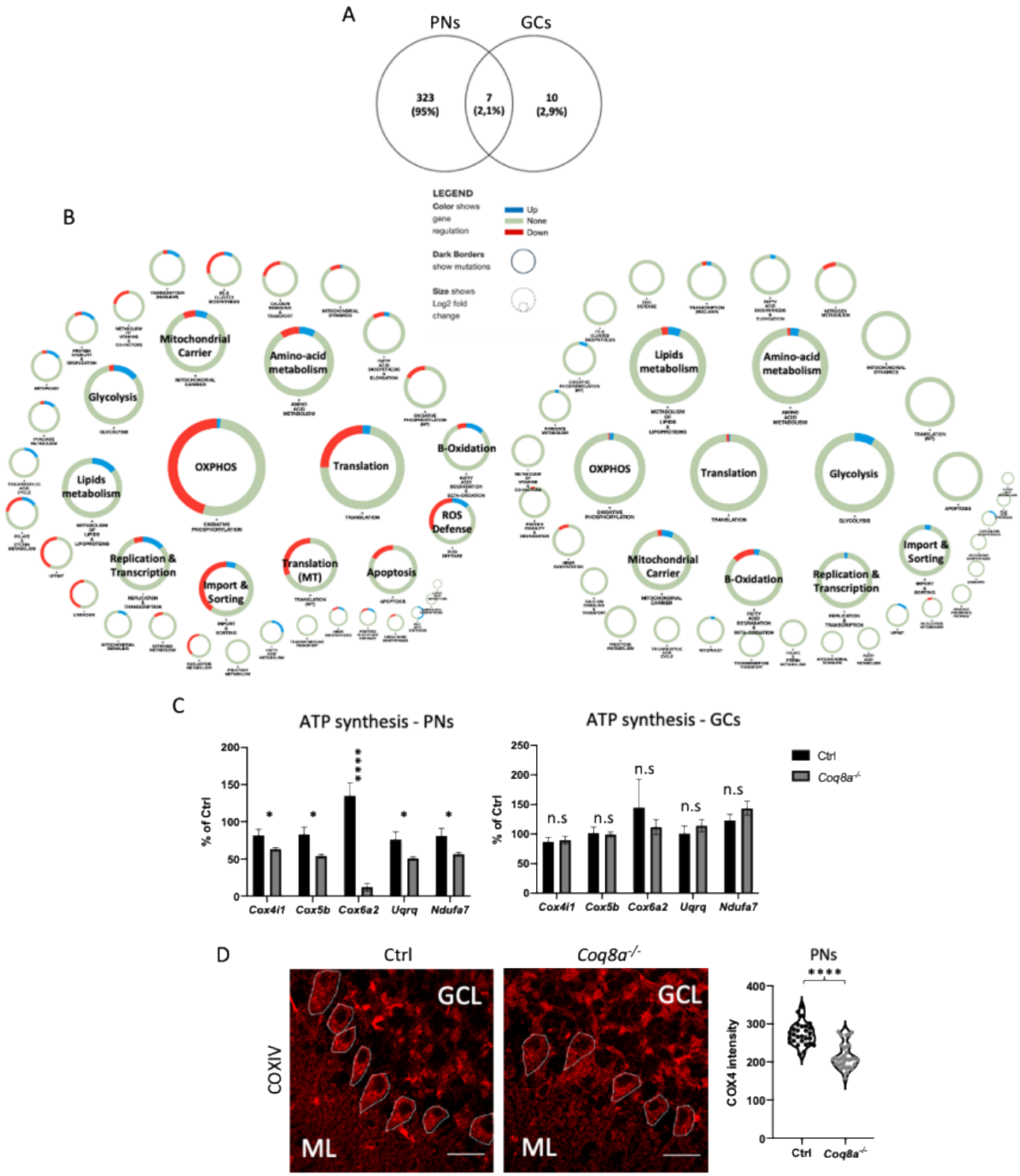
A
PNs
GCs
323 (95%)
7 (2,1%)
10 (2,9%)
B
LEGEND
Color shows gene regulation
Up
None
Down
Dark Borders show mutations
Size shows Log2 fold change
Mitochondrial Carrier
Amino-acid metabolism
Glycolysis
Lipids metabolism
OXPHOS
Translation
B-Oxidation
ROS Defense
Replication & Transcription
Translation (MT)
Apoptosis
Import & Sorting
C
ATP synthesis - PNs
ATP synthesis - GCs
% of Ctrl
Ctrl
Coq8a-/-
n.s
Cox4i1
Cox5b
Cox6a2
Uqrq
Ndufa7
D
Ctrl
Coq8a-/-
COXIV
GCL
ML
PNs
COX4 intensity

Figure 4.

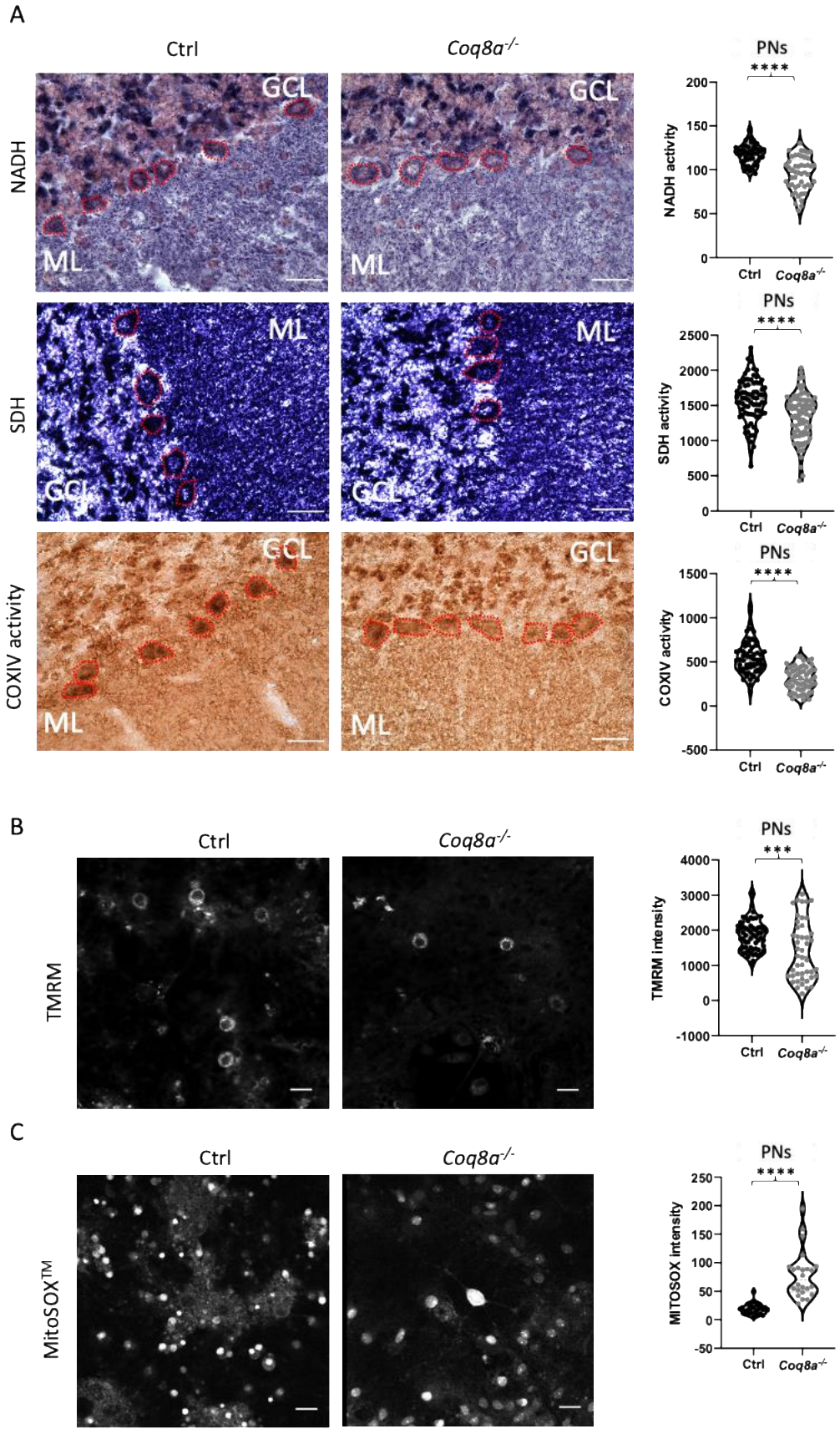
A
Ctrl
Coq8a-/-
NADH
SDH
COXIV activity
GCL
ML
PNs
****
NADH activity
SDH activity
COXIV activity
Ctrl
Coq8a-/-
B
TMRM
***
TMRM intensity
C
MitoSOX™
MITOSOX intensity

Figure 5.

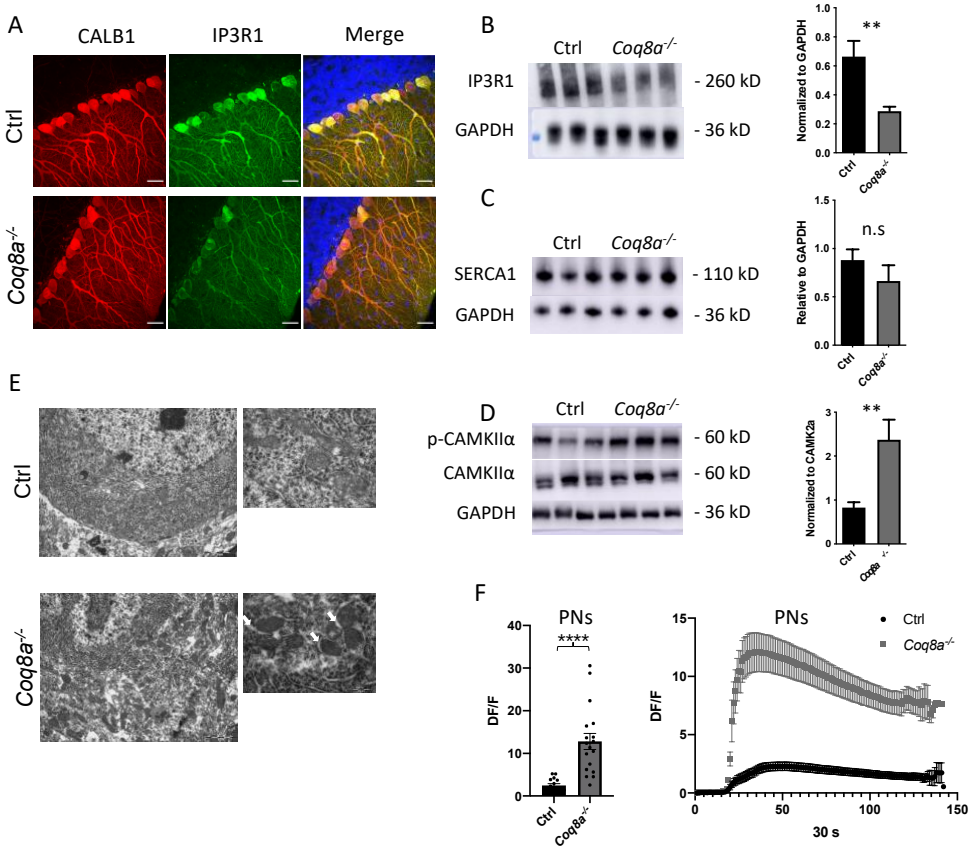
A
CALB1
IP3R1
Merge
Ctrl
Coq8a-/-
B
Ctrl
Coq8a-/-
IP3R1
- 260 kD
GAPDH
- 36 kD
Normalized to GAPDH
**
C
SERCA1
- 110 kD
n.s
Relative to GAPDH
D
p-CAMKIIα
- 60 kD
CAMKIIα
- 60 kD
Normalized to CAMK2a
E
F
PNs
****
DF/F
30 s

Figure 6.

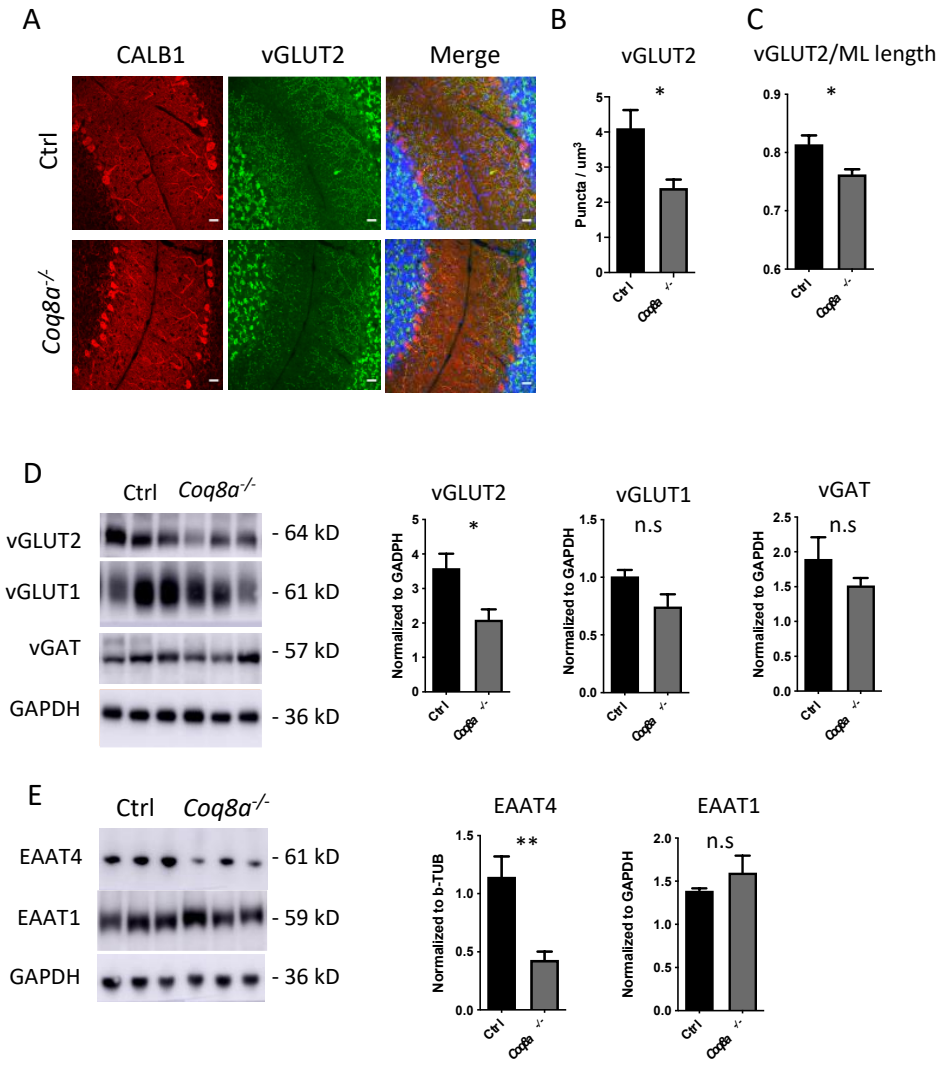
A
CALB1
vGLUT2
Merge
Ctrl
Coq8a-/-
B
vGLUT2
Puncta / um3
*
Ctrl
Coq8a -/-
C
vGLUT2/ML length
*
Ctrl
Coq8a -/-
D
Ctrl
Coq8a-/-
vGLUT2
vGLUT1
vGAT
GAPDH
- 64 kD
- 61 kD
- 57 kD
- 36 kD
vGLUT2
Normalized to GADPH
*
vGLUT1
n.s
vGAT
n.s
E
Ctrl
Coq8a-/-
EAAT4
EAAT1
GAPDH
- 61 kD
- 59 kD
- 36 kD
EAAT4
Normalized to b-TUB
**
EAAT1
n.s
Normalized to GAPDH

Figure 7.

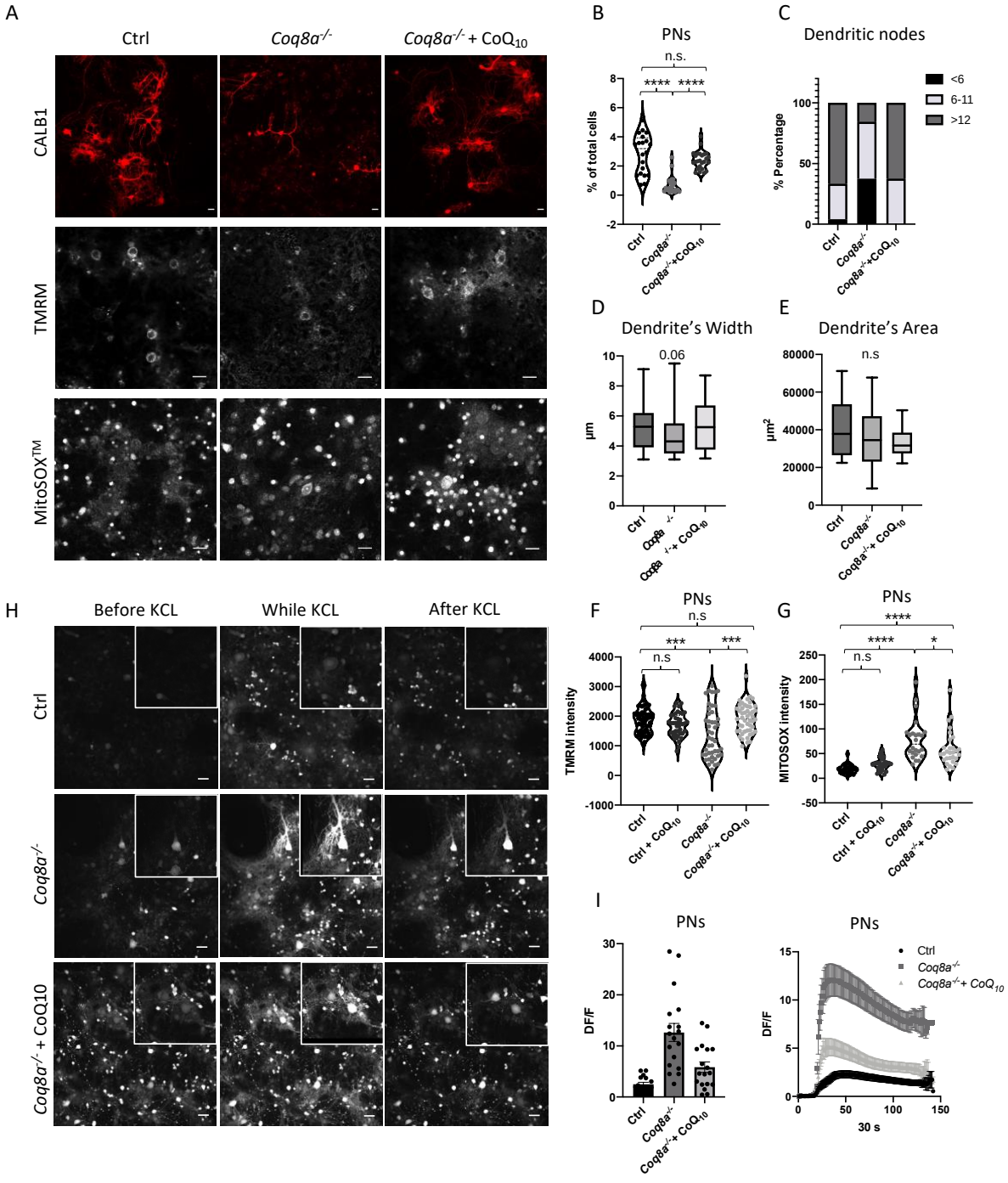
A
Ctrl
Coq8a-/-
Coq8a-/- + CoQ10
CALB1
TMRM
MitoSOX™
B
PNs
n.s.
****
****
% of total cells
Ctrl
Coq8a-/-
Coq8a-/-+CoQ10
C
Dendritic nodes
<6
6-11
>12
% Percentage
D
Dendrite's Width
0.06
µm
E
Dendrite's Area
n.s
µm2
H
Before KCL
While KCL
After KCL
Ctrl
Coq8a-/-
Coq8a-/- + CoQ10
F
PNs
n.s
***
***
n.s
TMRM intensity
Ctrl
Ctrl + CoQ10
Coq8a-/-
Coq8a-/- + CoQ10
G
PNs
****
****
*
n.s
MITOSOX intensity
I
PNs
DF/F
PNs
Ctrl
Coq8a-/-
Coq8a-/- + CoQ10
30 s

Disruption of the CoQ10 biosynthetic Complex Q causes mitochondrial dysfunction and neurodegeneration specifically in Purkinje neurons in COQ8A-ataxia.

Ioannis Manolaras[1-4], Laurence Reutenauer[1-6], Celine Keime[1-4], Aurelie Eisenmann[1-4], Olivier Griso[1-4], Bianca Habermann[7,8], Helene Puccio* [1-6].

[1]Départment de Médecine Translationnelle et Neurogénétique, Institut de Génétique et de Biologie Moléculaire et Cellulaire (IGBMC), Illkirch, France. [2]INSERM, U596, Illkirch, France. [3]CNRS, UMR7104, Illkirch, France. [4]Université de Strasbourg, Strasbourg, France. [5]INSERM U1217, Lyon, France. [6]CNRS UMR 5310. [7]Institut de Biologie du Développement de Marseille (IBDM). [8]CNRS, UMR7288, Marseille, France.

***Corresponding author:**

Hélène Puccio, current address: Institut NeuroMyoGene, UMR5310 INSERM U1217, Université Claude Bernard Lyon I, Faculté de Médecine, 8 avenue Rockefeller, 69008 Lyon France. helene.puccio@inserm.fr; Tel: +33-426-688-210.

Supplemental figures

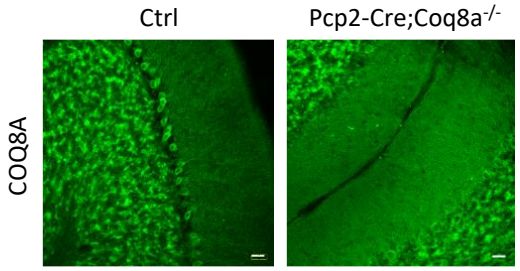

Figure S1. Specific deletion of COQ8A in PNs of Pcp2-Cre;Coq8a$^{L+/L+}$ mice. *Immunofluorescence using COQ8A antibody in sagittal cerebellar slices of Ctrl and Pcp2-Cre;Coq8a$^{L+/L+}$ mice. Scale at 25 µm.*

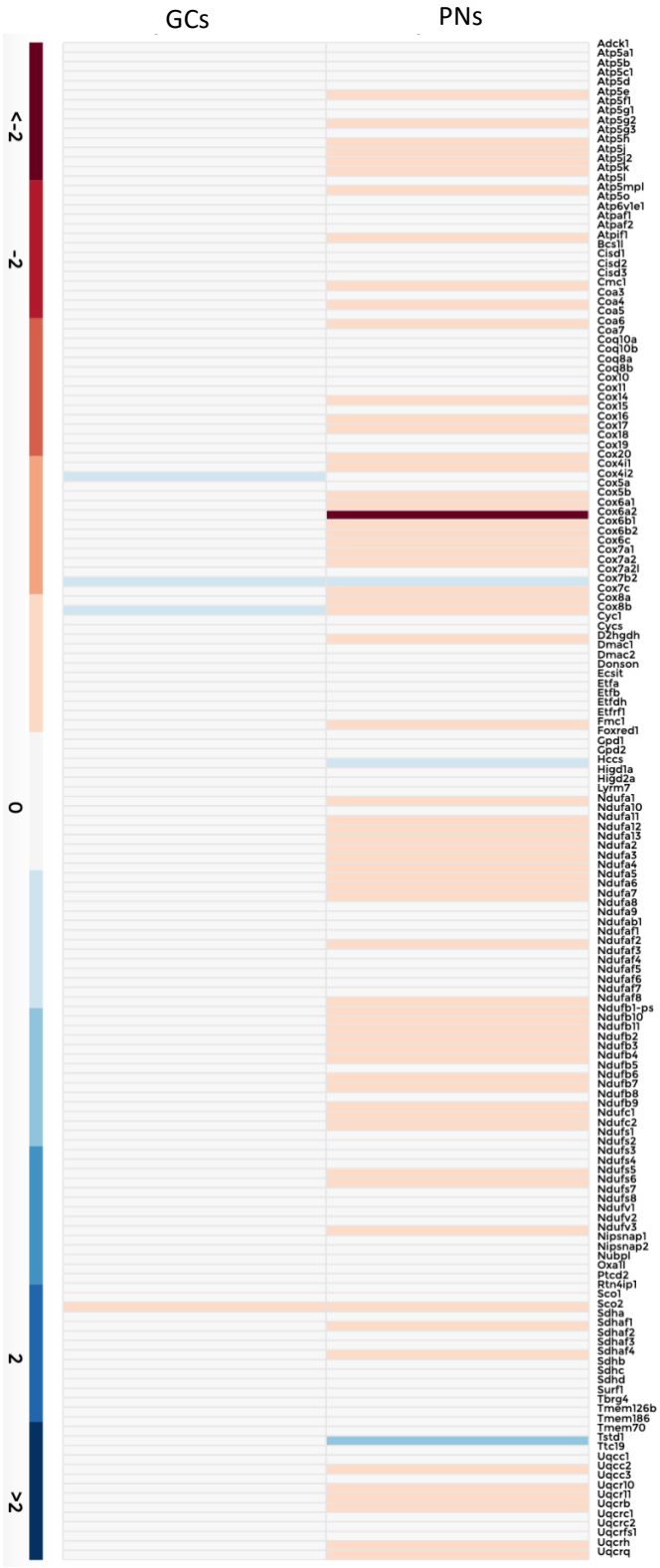

Figure S2. Heatmap comparison between Ctrl and Coq8a$^{-/-}$ PNs and GCs of transcripts involved in OXPHOS, using the online tool MitoXplorer for expression and interaction analysis of mitochondrial pathways.

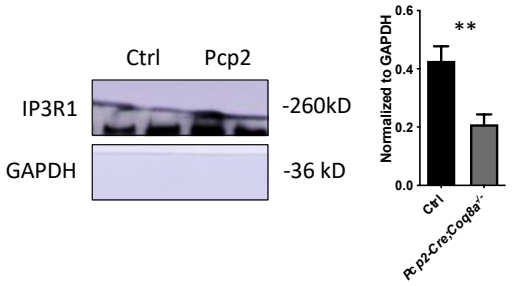

Figure S3. Decreased IP3R1 expression in Pcp2-Cre;Coq8a$^{L2+/L2+}$ mice*. Western blot for IP3R1 in Pcp2-cre;Coq8a$^{L2+/L2+}$ mice at 30 weeks of age (n=6, mean ± SEM, Student t test, **p-value < 0.01).*

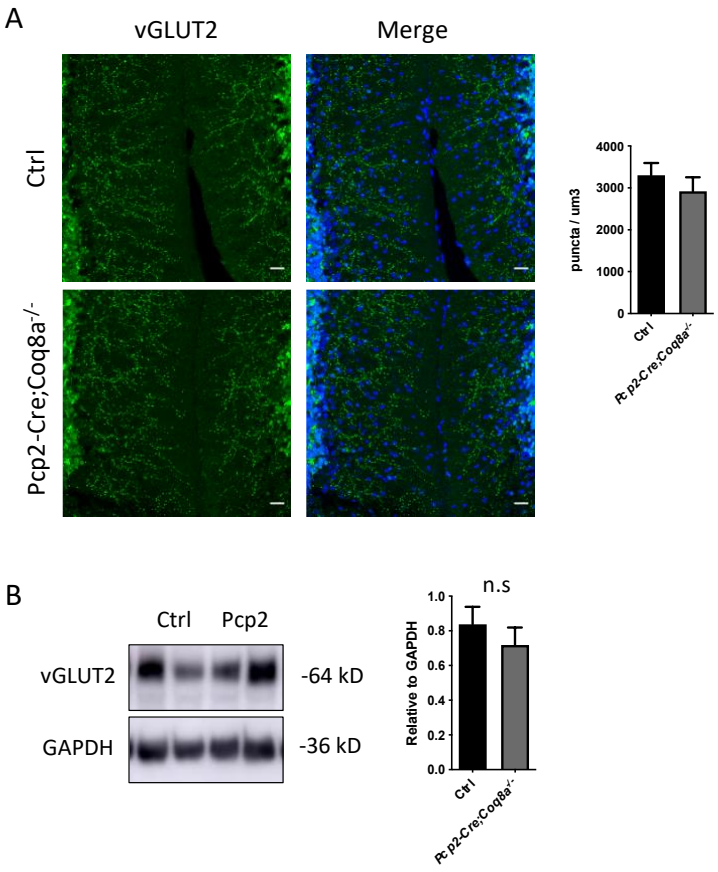

Figure S4. vGLUT2 expression and CF-PNs synapses in Pcp2-Cre;Coq8a$^{L2+/L2+}$ mice*. A) Immunofluorescence for vGLUT2 in the cerebellum of Pcp2-Cre;Coq8a$^{L2+/L2+}$ mice at 30 weeks (n=6, Scale bar = 25 μm). B) Western blot for vGLUT2 in Pcp2-Cre;Coq8a$^{L2+/L2+}$ mice at 30 weeks.*

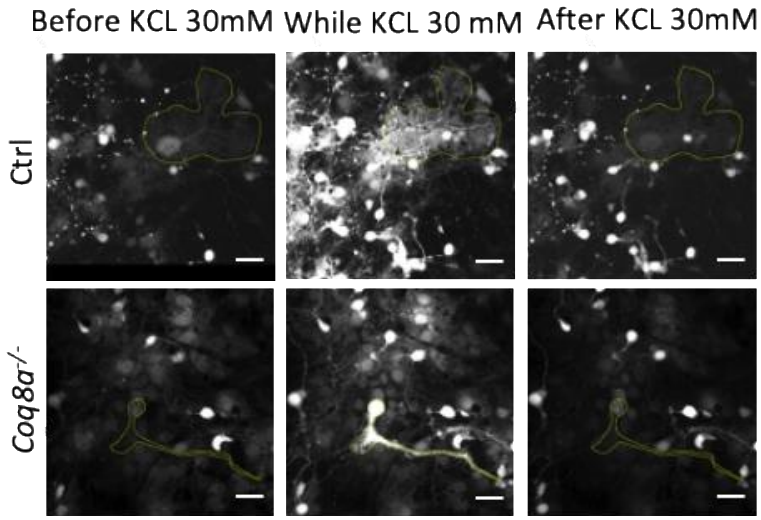

Figure S5. Live Ca^{2+} imaging in primary Coq8a$^{-/-}$ cerebellar cultures*. Live Ca^{2+} imaging using Calbryte520TM in primary Coq8a$^{-/-}$ cerebellar cultures at DIV21. Acquisitions indicate the Ca^{2+} response of the primary cultures before, during and after stimulation with 30 mM KCl. Ctrl and Coq8a$^{-/-}$ PNs are indicated. Scale bar = 25 µm*

Table S3. GO pathways analysis of the resulting transcripts from RNA-sequencing after LCM in PNs

Panther Panthways	# Represented	# present	Fold Enrichment	+/-	P value
SnRNP assembly	13	5	>20	+	3.66E-06
Cytochrome c to oxygen	9	3	>20	+	5.29E-04
Ubiquinol to Cytochrome c	7	2	>20	+	6.47E-03
ATP synthesis	36	6	>10	+	2.33E-05